Top quark spin and Htb interaction in charged Higgs and top quark associated production at LHC

Xue Gong,[1,*] Zong-Guo Si,[1,2,†] Shuo Yang,[3,‡] and Ya-juan Zheng[4,1,§]

[1]*School of Physics, Shandong University, Jinan, Shandong 250100, China*
[2]*Center for High Energy Physics, Peking University, Beijing 100871, China*
[3]*Physics Department, Dalian University, Dalian, 116622, China*
[4]*CASTS, CTS and Department of Physics, National Taiwan University, Taipei, China*

We study the charged Higgs production at LHC via its associated production with top quark. The kinematic cuts are optimized to suppress the background processes so that the reconstruction of the charged Higgs and top quark is possible. The angular distributions with respect to top quark spin are explored to study the Htb interaction at LHC.

PACS numbers: 14.80.Cp,14.65.Ha,12.60.-i

I. INTRODUCTION

The Standard Model (SM) of particle physics, with great success, is based on two cornerstone: gauge symmetry and electroweak spontaneous symmetry breaking mechanism (EWSB). The gauge group $SU(3)_C \times SU(2)_L \times U(1)_Y$ of the SM has been confirmed by the discovery of W/Z bosons and lots of precision measurements. As the other cornerstone, the mechanism of EWSB is implemented by introducing only one complex Higgs doublet Φ in the SM and then trigging the electroweak symmetry breaking after the neutral component of Φ developing a vacuum expectation. In the meanwhile, the masses of weak gauge bosons and fermions are generated. In the SM, there is only one physical neutral Higgs boson H after EWSB. The discovery of the Higgs boson will help to unveil the mysteries of EWSB and mass generation of SM particles. Recently, one Higgs-like particle around 126 GeV has been discovered at LHC by ATLAS and CMS collaborations[1, 2]. It is important to further confirm the identity of this particle. In SM, only one complex scalar doublet is introduced based on the "minimal principle". It is natural to consider more complex scalar sector, for example, the two Higgs doublet structure. Especially, there are many motivations to study the two Higgs doublet model (2HDM). Such as, in the supersymmetric models, a single Higgs doublet is unable to give mass simultaneously to the charge 2/3 and charge -1/3 quarks and the anomaly cancelation also require additional Higgs doublet. Another motivation for 2HDM is that it could generate a baryon asymmetry of the universe of sufficient size. Interestingly, ATLAS and CMS announced that there is an enhancement in the di-photon channel of Higgs decay $h \to \gamma\gamma$ [1, 2]. This enhancement can be explained by charged Higgs from 2HDM[3].

There are many scenarios in 2HDM structure [4, 5]. Without imposing discrete symmetries, the 2HDM suffers serious flavour changing neutral currents (FCNC) at tree-level. For the suppression of leading order FCNC as well as CP violation in the Higgs sector, we consider CP-conserving 2HDMs with extra discrete symmetry. Popular Type I and II 2HDM belong to this kind. As one of the minimal extensions of the SM, 2HDM [4, 5], has five physical Higgs scalars after the spontaneous symmetry breaking, i.e., two neutral CP-even bosons h_0 and H_0, one neutral CP-odd boson A, and two charged bosons $H^\pm$. In diverse models, different scalar multiplets and singlets could generate neutral scalars and there exists mixing between neutral scalars which make it difficult to unentangle the Higgs properties and confirm the existence of extended Higgs sector. However, the discovery of the charged Higgs boson could provide an unambiguous signature of the extended Higgs sector and help to further distinguish models.

Motivated by above reasons, the charged Higgs $H^\pm$ has been searched for in many years at colliders. One model-independent direct limit from the LEP experiments which gives $M > 78.6$ GeV at 95% C.L. where M represents the mass of charged Higgs by exclusive decay channels of $H^+ \to c\bar{s}$ and $H^+ \to \tau^+\nu$[6]. At hadron colliders, the search approaches for the charged Higgs are different in low mass range $M < m_t$ and in large mass range $M > m_t$. In the low mass range $M < m_t - m_b$, the search for the signal mainly focus on the top quark decay $t \to H^+ b$ followed by decay mode $H^+ \to \bar{\tau}\nu$. On the other hand, for large mass range $M > m_t + m_b$, the signal is from the dominant production process, the gb fusion process $gb \to tH^-$, followed by dominant decay modes $H^- \to t\bar{b}$ and $H^- \to \tau\bar{\nu}$. The Tevatron

*Electronic address: gongxue@mail.sdu.edu.cn
†Electronic address: zgsi@sdu.edu.cn
‡Electronic address: yangshuo@dlu.edu.cn
§Electronic address: yjzheng218@gmail.com

has put a constraint to 2HDM on the small $\tan\beta$ and large $\tan\beta$ regions for a charged Higgs boson with mass up to ~ 160 GeV [7]. In addition, the indirect constraints can be extracted from B-meson decays since the charged Higgs contributes to the FCNC at one loop level. In Type II 2HDM, a limit on the charged Higgs mass $M > 316$ GeV at 95% C.L. is obtained dominantly from $b \to s\gamma$ branching ratio measurement irrespective of the value of $\tan\beta$ [8]. However, in Type III or general 2HDM the phases of the Yukawa couplings are free parameters so that M can be as low as 100 GeV[9]. More detailed discussions on phenomenological constraints on charged Higgs, we refer to Ref. [10].

Along with the experimental search for the charged Higgs boson, extensive phenomenological studies on charged Higgs boson production have been carried out [11–18]. Especially, the gb fusion process $gb \to tH^-$ for $M > m_t + m_b$ [13–19] has drawn more attentions due to the large couplings of Htb interaction.

In this work, we revisit this process at the LHC and take a method similar to Ref. [20] to distinguish the signal from backgrounds. As demonstrated in Ref. [20], the angular distribution related to top quark spin is efficient to suppress background and disentangle the chiral coupling of the W' boson to SM fermions. Here, we choose the angular distributions of the top quark and the lepton resulting from top and charged Higgs decay to disentangle Htb couplings at LHC.

This paper is organized as follows. In Section II., the corresponding theoretical framework is briefly introduced. Section III. is devoted to the numerical analysis of top quark and charged Higgs associated production. Specifically, the correlated angular distributions are investigated to identify the interaction of top-bottom quark and charged Higgs. Finally, a short summary is given.

II. THEORETICAL FRAMEWORK

A. Lagrangian related to the interaction of Higgs and quarks

We start with a brief introduction to the two-Higgs-Doublet Model (2HDM) which is one of the minimal extensions of SM. Different from SM, 2HDM involves two complex $SU(2)_L$ doublet scalar fields.

$$\Phi_i = \begin{pmatrix} H_i^+ \\ (H_i^0 + iA_i^0)/\sqrt{2} \end{pmatrix}, \tag{1}$$

where $i = 1, 2$. Imposing CP invariance and $\mathrm{U(1)_{EM}}$ gauge symmetry, the minimization of potential gives

$$\langle\Phi_i\rangle = \frac{1}{\sqrt{2}}\begin{pmatrix} 0 \\ v_i \end{pmatrix},$$

with v_i $(i = 1, 2)$ are non-zero vacuum expectation value (VEV). One important parameter in 2HDMs $\tan\beta \equiv v_2/v_1$ is defined accordingly, which determines the interactions of the various Higgs fields with the vector bosons and with the fermions, thus has substantial meaning in discussing phenomenology. The most severe constraints on $\tan\beta$ and M come from flavour physics including B and D mesons, ΔM_{B_d}, $b \to s\gamma$ and $Z \to b\bar{b}$[8, 21]. Large $\tan\beta$ is favored by B meson rare decays[22–24]. Specifically, for the Type II model, the upper bound on $\tan\beta$ from $D_s \to \tau\nu_\tau$ is $\tan\beta \leq 50$ with charged Higgs mass $M = 600$ GeV [3].

In this work we aim to study the charged Higgs phenomenology with large $\tan\beta$ and choose the Type II Yukawa couplings as the working model

$$\begin{aligned} -\mathcal{L} \;=\; & -\cot\beta\frac{m^u}{v}\bar{u}_L(H+iA)u_R - \cot\beta\frac{m^u}{v}\bar{u}_R(H-iA)u_L \\ & +\tan\beta\frac{M^d}{v}\bar{d}_L(H-iA)d_R + \tan\beta\frac{M^d}{v}\bar{d}_R(H+iA)d_L \\ & -\sqrt{2}\cot\beta\frac{M^u}{v}V_{ud}^\dagger\bar{d}_L H^- u_R - \sqrt{2}\tan\beta\frac{M^d}{v}V_{ud}^\dagger\bar{d}_R H^- u_L \\ & -\sqrt{2}\cot\beta\frac{M^u}{v}V_{ud}\bar{u}_R H^+ d_L - \sqrt{2}\tan\beta\frac{M^d}{v}V_{ud}\bar{u}_L H^+ d_R. \end{aligned} \tag{2}$$

The VEV of SM Higgs is related as $v = \sqrt{v_1^2 + v_2^2}$. $t\bar{b}H^-$ vertex given in Ref.[4] can be written as

$$g_{H^- t\bar{b}} = \frac{g}{2\sqrt{2}m_W}[m_t\cot\beta(1+\gamma_5) + m_b\tan\beta(1-\gamma_5)] = g_a + g_b\gamma_5 \tag{3}$$

with $g_{a,b} = g_{\mathrm{W}}(\tan\beta m_b \pm \cot\beta m_t)/(2\sqrt{2}m_{\mathrm{W}})$. In the specific discussions below in Sec. III, we will consider various combinations of g_a and g_b accordingly.

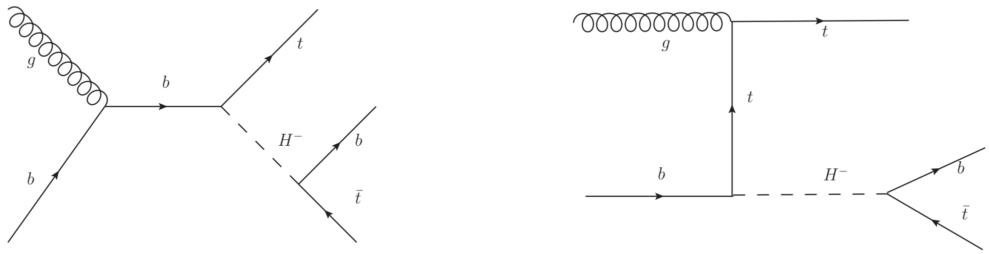

FIG. 1: Feynman diagrams for $gb \to tH^- \to t\bar{t}b$ process.

B. Charged Higgs production associated with single top quark at hadron colliders

We begin to consider the following processes(Fig. 1)

$$g(p_1) + b(p_2) \to t(p_3, s_t) + H^-(p_4) \to t(p_3, s_t) + b(p_5) + \bar{t}(p_6, s_{\bar{t}}), \tag{4}$$

where p_i denotes the 4-momentum of the corresponding particle. $s_t(s_{\bar{t}})$ is the (anti-)top quark spin in 4-dimension and $s_t^2 = s_{\bar{t}}^2 = -1$, $p_3 \cdot s_t = p_6 \cdot s_{\bar{t}} = 0$.

Under the narrow width approximation of the charged Higgs, i.e., the charged Higgs produced on-shell,

$$\lim_{\Gamma \to 0} \frac{1}{(p_4^2 - M^2)^2 + \Gamma^2 M^2} \longrightarrow \frac{\pi}{\Gamma M} \delta(p_4^2 - M^2), \tag{5}$$

where Γ and M respectively denote the decay width and mass of the charged Higgs boson, the matrix element squared including top quark spin information for the process (4) can be written as follows

$$|\mathcal{M}(s_t, s_{\bar{t}})|^2 = \frac{\pi}{\Gamma M} |\mathcal{M}_{gb \to tH^-}(s_t)|^2 \, |\mathcal{M}_{H^- \to b\bar{t}}(s_{\bar{t}})|^2 \, \delta(p_4^2 - M^2), \tag{6}$$

where

$$|\mathcal{M}_{gb \to tH^-}(s_t)|^2 = \frac{g_s^2}{2N_c} \Big\{ \mathcal{A} + \mathcal{B}_1(p_1 \cdot s_t) + \mathcal{B}_2(p_2 \cdot s_{\bar{t}}) \Big\}, \tag{7}$$

$$|\mathcal{M}_{H^- \to b\bar{t}}(s_{\bar{t}})|^2 = (g_a^2 + g_b^2)(M^2 - m_b^2 - m_t^2) - 2(g_a^2 - g_b^2) m_b m_t - 4 g_a g_b m_t (p_5 \cdot s_{\bar{t}}). \tag{8}$$

The formula for $\mathcal{A}$, $\mathcal{B}_1$ and $\mathcal{B}_2$ are listed in the following

$$\mathcal{A} = (g_a^2 + g_b^2)\, A_1 + m_b m_t (g_b^2 - g_a^2)\, A_2, \tag{9}$$

with

$$\begin{aligned} A_1 &= \frac{\hat{s}(p_1 \cdot p_3) - m_b^2(4p_1 \cdot p_3 + 3p_2 \cdot p_3)}{(\hat{s} - m_b^2)^2} + \frac{\hat{s}(p_1 \cdot p_3) + m_t^2(\hat{s} - 2p_2 \cdot p_3)}{4(p_1 \cdot p_3)^2} \\ &\quad - \frac{m_t^2(\hat{s} - 2m_b^2) - 2(p_1 \cdot p_3) m_b^2 + 2(\hat{s} - 2p_2 \cdot p_3)(p_1 \cdot p_3 + p_2 \cdot p_3)}{2(p_1 \cdot p_3)(\hat{s} - m_b^2)} \end{aligned} \tag{10}$$

$$A_2 = \frac{(\hat{s} + 2m_b^2)}{(\hat{s} - m_b^2)^2} + \frac{m_t^2 - p_1 \cdot p_3}{2(p_1 \cdot p_3)^2} - \frac{2p_1 \cdot p_3 + 4p_2 \cdot p_3 - \hat{s}}{2(p_1 \cdot p_3)(\hat{s} - m_b^2)} \tag{11}$$

and

$$B_1 = 2 g_a g_b m_t \Big[\frac{4m_b^2 - \hat{s}}{(\hat{s} - m_b^2)^2} + \frac{2p_2 \cdot p_3 - \hat{s}}{4(p_1 \cdot p_3)^2} + \frac{1}{p_1 \cdot p_3} - \frac{p_2 \cdot p_3}{(p_1 \cdot p_3)(\hat{s} - m_b^2)} \Big], \tag{12}$$

$$B_2 = 2 g_a g_b m_t \Big[\frac{3m_b^2}{(\hat{s} - m_b^2)^2} + \frac{m_t^2 - p_1 \cdot p_3}{2(p_1 \cdot p_3)^2} + \frac{\hat{s} - p_1 \cdot p_3 - 2p_2 \cdot p_3}{(p_1 \cdot p_3)(\hat{s} - m_b^2)} \Big]. \tag{13}$$

(14)

Obviously, the top quark spin effects which are related to the product $(g_a g_b)$ disappear for a pure scalar or pseudo-scalar charged Higgs boson. The matrix element squared for the process $g\bar{b} \to \bar{t}H^+ \to t\bar{t}\bar{b}$ can be obtained from the above equations by using CP-invariance. The spin density matrix for the subsequent polarized top quark decays can be found in Ref.[25].

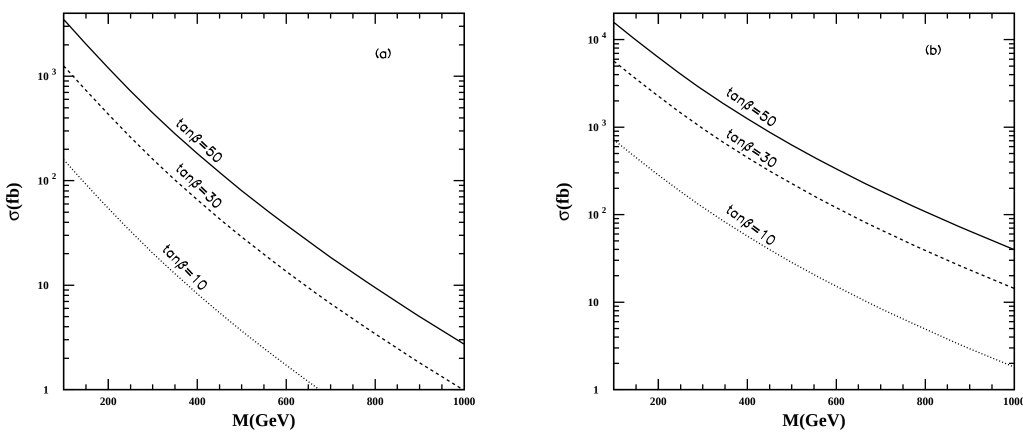

FIG. 2: The total cross section as a function of M for $pp \to tH^-$ process at LHC for (a) 8 TeV and (b) 14 TeV.

III. NUMERICAL RESULTS AND DISCUSSION

For the processes $pp \to tH^-$, the total cross section can be expressed as

$$\sigma = \int f_g(x_1) f_b(x_2) \hat{\sigma}_{gb \to tH^-}(x_1 x_2 s) dx_1 dx_2, \tag{15}$$

where $f_g(x_1)(f_b(x_2))$ is the parton distribution function(PDF) of gluon(quark), $\sqrt{s}$ is the center of mass energy (*c.m.*) of parton-parton collision, and $\hat{\sigma}$ is the partonic level cross section for $gb \to tH^-$ process. In our numerical calculations we set $V_{tb} = 1$, $M_W = 80.399$ GeV, $m_b = 4.70$ GeV and $m_t = 173.1$ GeV. For PDF, we use CTEQ6L1[26]. In Fig. 2, the total cross sections for the process $pp \to tH^-$ are shown as a function of charged Higgs mass for $\tan\beta = 10$, 30, and 50 in 2HDM at the LHC with 8 TeV and 14 TeV. Obviously the tH^- production rate at 14 TeV is much higher than that at 8 TeV.

In the following, we respectively investigate the processes

$$pp \to tH^- \to t\bar{t}b \to bl^+ + b\bar{b}jj + \not{E}_T, \tag{16}$$

$$pp \to tH^- \to t\bar{t}b \to bjj + b\bar{b}l^- + \not{E}_T. \tag{17}$$

In process (16), the top quark produced associated with H^- decays semi-leptonically, and the anti-top quark from charged Higgs decays hadronically, i.e., $t \to bl^+\nu_l$ and $\bar{t} \to \bar{b}jj$. While in process (17), $t \to bjj$ and $\bar{t} \to \bar{b}l^-\bar{\nu}_l$. The charged lepton can be used to trigger the event. The dominant background for the above processes is $pp \to t\bar{t}j$ events.

To be more realistic, the simulation at the detector is performed by smearing the leptons and jets energies according to the assumption of the Gaussian resolution parameterization

$$\frac{\delta(E)}{E} = \frac{a}{\sqrt{E}} \oplus b, \tag{18}$$

where $\delta(E)/E$ is the energy resolution, a is a sampling term, b is a constant term, and $\oplus$ denotes a sum in quadrature. We take $a = 5\%$, $b = 0.55\%$ for leptons and $a = 100\%$, $b = 5\%$ for jets respectively[27].

For our signal process, one top quark which decays hadronically can be reconstructed from the three jets by demanding $|M_{jjj} - m_t| \leq 30$GeV, while to reconstruct another top that is leptonically decay, the 4-momentum of the neutrino should be known. But the neutrino is an unobservable particle, so we have to utilize kinematical constraints to reconstruct its 4-momentum. Its transverse momentum can be obtained by momentum conservation from the observed particles

$$\mathbf{p}_{\nu T} = -(\mathbf{p}_{lT} + \sum_{j=1}^{5} \mathbf{p}_{jT}), \tag{19}$$

while its longitudinal momentum can not be determined in this way due to the unknown boost of the partonic *c.m.* system. Alternatively, it can be solved with twofold ambiguity through the on shell condition for the W-boson

$$m_W^2 = (p_\nu + p_l)^2. \tag{20}$$

Furthermore one can remove the ambiguity through the reconstruction of another top quark. For each possibility we evaluate the invariant mass

$$M_{jl\nu}^2 = (p_l^2 + p_\nu + p_j)^2, \tag{21}$$

where j refers to the any one of the two left jets and pick up the solution which is closest to the top quark mass. With such a solution, one can reconstruct the 4-momentum of the neutrino and that of another top quark.

In our following numerical calculations, we apply the basic acceptance cuts(referred to as cut I)

$$\begin{aligned}
&p_{lT} > 20 \text{ GeV}, \quad p_{jT} > 20 \text{ GeV}, \quad \not{E}_T > 20 \text{ GeV}, \\
&|\eta_l| < 2.5, \quad |\eta_j| < 2.5, \quad \Delta R_{jj(lj)} > 0.4, \\
&|M_{j_a l\nu} - m_t| \leq 30 \text{ GeV}, \quad |M_{j_b j_c j_d} - m_t| \leq 30 \text{ GeV}, \quad |M_{j_b j_c} - m_W| < 10 \text{ GeV}.
\end{aligned} \tag{22}$$

To purify the signal, we further adopt the following cuts:

- Cut II: $|M_{jj_bj_cj_d} - M| \leq 10\%\, M$ or $|M_{jj_al\nu} - M| \leq 10\%\, M$.
- Cut III: We demand the remaining jet that cannot be used to reconstruct top quarks to be b-jet.

The b-tagging efficiency is assumed to be 60% while the miss-tagging efficiency of a light jet as a b jet is taken as transverse momentum dependent [27]:

$$\epsilon_l = \begin{cases} \dfrac{1}{150}, & P_T < 100\,\text{GeV}, \\ \dfrac{1}{450}\left[\dfrac{P_T}{25\,\text{GeV}} - 1\right], & 100\,\text{GeV} \leq P_T < 250\,\text{GeV}, \\ \dfrac{1}{50}, & P_T \geq 250\,\text{GeV}. \end{cases} \tag{23}$$

In Fig. 3, we display the distributions with respect to the invariant mass between the reconstructed top(antitop) and the remaining jet, i.e, $1/\sigma(d\sigma/dM_{tb} + d\sigma/dM_{\bar{t}\bar{b}})$ after cut I at LHC. The cross sections for the signal processes (16) and (17) with $\tan\beta = 30$ and different charged Higgs mass after each cuts at LHC 8 and 14 TeV are respectively listed in Table. I and Table. II. The dominant SM background related to the signal is $pp \to t\bar{t}j \to l^\pm + 5jets + \not{E}_T$ process. We employ MadEvent[28] to simulate the background processes. The other SM background processes, eg, $Wjjjjj$, $WWjjj$ and $WZjjj$, etc. are dramatically reduced by the acceptance cuts we adopted and therefore we neglected them here. Supposing the integral luminosity to be 20 fb^{-1} at $\sqrt{s} = 8$ TeV, one can notice that it is difficult for the charged Higgs associated with a top quark to be detected when its mass is above 500 GeV. While with $300fb^{-1}$ integral luminosity at 14 TeV, the tH^- production is easier to be observed. Detailed analysis shows that for $pp \to tH^- \to t\bar{t}b \to l^+(or\ l^-) + bb\bar{b}jj + \not{E}_T$ process at 14 TeV , the significance of signal to background can also be above three sigma for the charged Higgs mass $M \leq 1$ TeV. Therefore, in the following, we will focus on investigating the angular distributions for the processes (16) and (17) at $\sqrt{s} = 14$ TeV with $\tan\beta = 30$.

From Eqs. (7) and (8), one can notice that top quark spin effect is related to the product of the coupling g_a and g_b. Use the same method as in ref.[29], we find that this kind of top quark spin effects can be translated into the angular distributions of the charged leptons. Here corresponding to the process (16) and (17), we respectively introduce two kinds of angular distributions

$$\frac{1}{\sigma}\frac{d\sigma}{d\cos\theta^*} = \frac{1}{2}[1 + A_{FB}\cos\theta^*], \quad \frac{1}{\sigma}\frac{d\sigma}{d\cos\bar{\theta}^*} = \frac{1}{2}[1 + \bar{A}_{FB}\cos\bar{\theta}^*], \tag{24}$$

where

$$\cos\theta^* = \frac{\mathbf{p}_{l^+}^* \cdot \mathbf{p}_t^*}{|\mathbf{p}_{l^+}^*||\mathbf{p}_t^*|}, \qquad \cos\bar{\theta}^* = \frac{\mathbf{p}_{l^-}^* \cdot \mathbf{p}_{\bar{t}}^*}{|\mathbf{p}_{l^-}^*||\mathbf{p}_{\bar{t}}^*|}. \tag{25}$$

Here $\mathbf{p}_{l^+}^*$ is the 3-momentum of charged lepton in the top quark rest frame $\mathbf{p}_t^*$ is the 3-momentum of the top quark in tH^- *c.m.* frame. While $\mathbf{p}_{l^-}^*$ is the 3-momentum of charged lepton in the anti-top quark rest frame $\mathbf{p}_{\bar{t}}^*$ is the 3-momentum of the anti-top quark in the charged Higgs rest frame. A_{FB} and $\bar{A}_{FB}$ in eq.(24) can be determined by

$$A_{FB} = \frac{\sigma(cos\theta^* > 0) - \sigma(cos\theta^* < 0)}{\sigma(cos\theta^* > 0) + \sigma(cos\theta^* < 0)}, \qquad \bar{A}_{FB} = \frac{\sigma(cos\bar{\theta}^* > 0) - \sigma(cos\bar{\theta}^* < 0)}{\sigma(cos\bar{\theta}^* > 0) + \sigma(cos\bar{\theta}^* < 0)}. \tag{26}$$

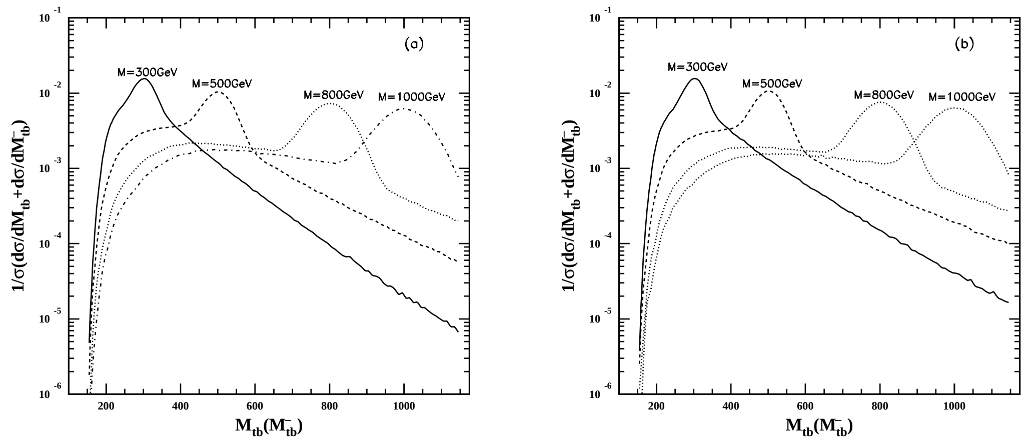

FIG. 3: The distributions $1/\sigma(d\sigma/dM_{tb} + d\sigma/dM_{\bar{t}b})$ with respect to the invariant mass between the reconstructed top(antitop) and the remaining jet after cut I at LHC.

These observables reflect the Htb interaction. In the following we will investigate the angular distributions for three different combinations of g_a and g_b

- $(g_a g_b) > 0$, eg., $g_a = \pm g_{\rm W}(\tan\beta m_b + \cot\beta m_t)/(2\sqrt{2}m_{\rm W})$, $g_b = \pm g_{\rm W}(\tan\beta m_b - \cot\beta m_t)/(2\sqrt{2}m_{\rm W})$.
- $(g_a g_b) = 0$, eg., $g_a = 0$, $g_b = g_{\rm W}(\tan\beta m_b - \cot\beta m_t)/(2\sqrt{2}m_{\rm W})$ or $g_a = g_{\rm W}(\tan\beta m_b + \cot\beta m_t)/(2\sqrt{2}m_{\rm W})$, $g_b = 0$.
- $(g_a g_b) < 0$, eg., $g_a = \pm g_{\rm W}(\tan\beta m_b + \cot\beta m_t)/(2\sqrt{2}m_{\rm W})$, $g_b = \mp g_{\rm W}(\tan\beta m_b - \cot\beta m_t)/(2\sqrt{2}m_{\rm W})$.

The charged lepton angular distributions with respect to $\cos\theta^*$ and $\cos\bar{\theta}^*$ before and after all cuts are respectively shown in Figs. 4 and 5. The related predictions for A_{FB} and $\bar{A}_{FB}$ are listed in table III. Due to the fact that the contribution from the s-channel(Fig.1(a)) decreases as the charged Higgs mass increases, before all the acceptance cuts, the $\cos\theta^*$ distribution and the related results for A_{FB}, which are related to tH^- production also depends on M, while the $\cos\bar{\theta}^*$ distribution and the related results for $\bar{A}_{FB}$, which are related to the charged Higgs decay do not depend on M. The $\cos\theta^* = -1(\cos\bar{\theta}^* = -1)$ region corresponds to leptons that are emitted into the hemisphere opposite to the (anti)top direction of flight in the tH^- *c.m.* frame. These leptons are therefore less energetic on average and thus more strongly affected by the acceptance cuts than those in the remaining region[30]. Therefore the presence of the acceptance cuts severely distort these distributions in the vicinity of $\cos\theta^* = -1(\cos\bar{\theta}^* = -1)$ region as shown in Figs. 4 and 5. Therefore for A_{FB} and $\bar{A}_{FB}$ after all acceptance cuts, we choose $\cos\theta$ ranges from -0.5 to 0.5. It seems that after the acceptance cuts, the angular distribution with respect to $cos\theta^*(\cos\bar{\theta}^*)$ and $A_{FB}(\bar{A}_{FB})$ is more helpful to investigate the Htb interactions for light(heavy) charged Higgs production associated with top quark at LHC.

IV. SUMMARY

The observation of charged Higgs would be an unambiguous signal for the existence of new physics beyond SM. Therefore it is important to study the related phenomena both at theory and experiments. In this paper, we study the tH^- associated production via $pp \to tH^- \to t\bar{t}b \to l^\pm + bb\bar{b}jj + \not{E}_T$ process at LHC. It is found that with 300 fb^{-1} integral luminosity at $\sqrt{s} = 14$ TeV, the signal can be distinguished from the backgrounds for the charged Higgs mass up to 1TeV or even larger. If the tH^- production is observed at LHC, one of the key questions is to identify the Htb interaction. For this aim, we investigate the angular distributions of the charged leptons and the related forward-backward asymmetry induced by top quark spin. It is found that these distributions and observables are sensitive to the product of g_a and g_b so that they can be used to identify the Htb interaction. Though further studies are still necessary both at theory and experiments, the Htb interaction can be studied by the help of the charged lepton angular distribution and the related forward-backward asymmetry in the charged Higgs and top quark associated production at LHC.

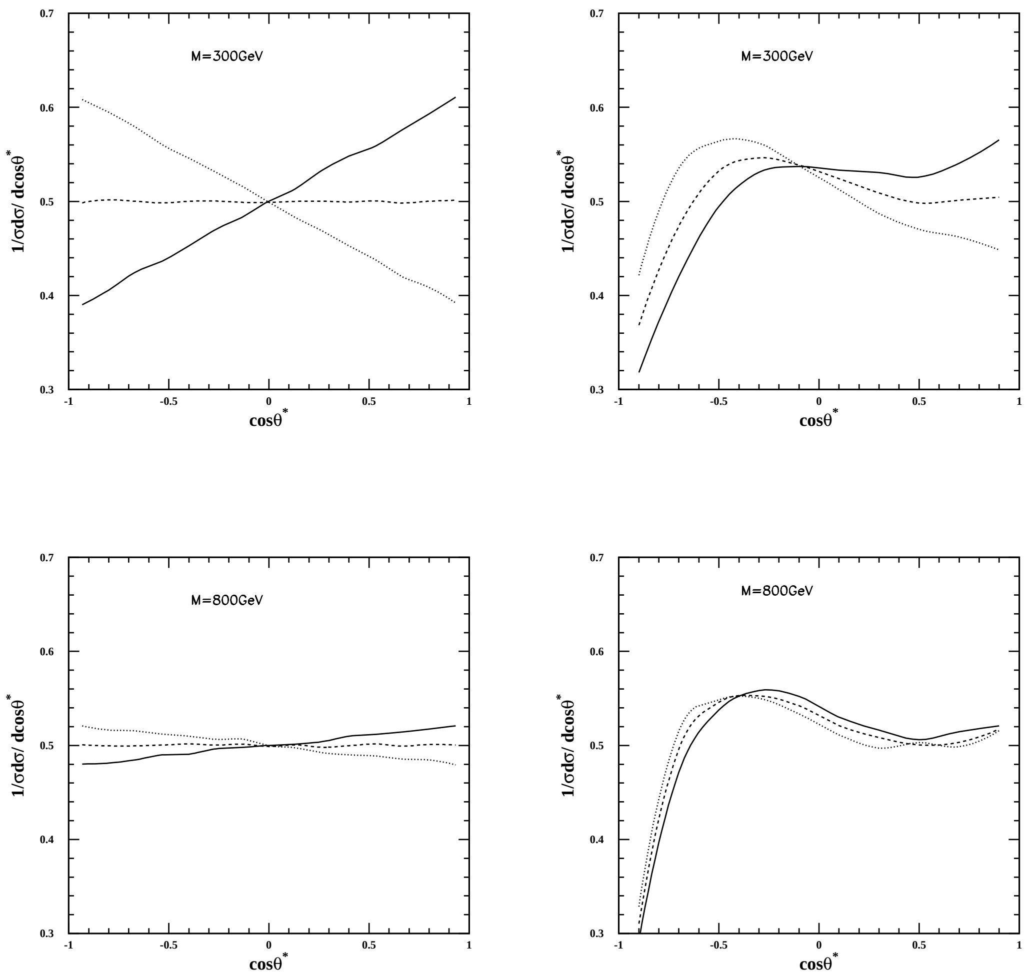

FIG. 4: The angle distribution of the charged lepton for $M = 300$, 800 GeV with nocut and all cuts at $\sqrt{s} = 14$ TeV respectively for the process of $pp \to tH^- \to l^+ + 5jets + \not{E}_T$.The solid line represents $(g_a g_b) > 0$. The dashed line represents $(g_a g_b) = 0$. The dotted line represents $(g_a g_b) < 0$.

Signal	$\sigma(pp \to tH^- \to t\bar{t}b \to l^\pm + 5jets + \not{E}_T)$ (fb)			
M(TeV)	0.3	0.5	0.8	1.0
No cuts	45.18	8.62	1.02	0.30
Cut I	11.72	2.20	0.25	0.07
+Cut II	9.59	1.73	0.20	0.05
+Cut III	5.76	1.04	0.12	0.03
Background	$\sigma(pp \to t\bar{t}j \to l^\pm + 5jets + \not{E}_T)$ (fb)			
Cuts I+II+III	10.25	3.85	0.97	0.46
S/B	0.56	0.27	0.12	0.07
$S/\sqrt{B}$	8.05	2.37	0.54	0.20

TABLE I: The cross section of the signal process $pp \to tH^- \to l^\pm + 5jets + \not{E}_T$ and the background process of $pp \to t\bar{t}j \to l^\pm + 5jets + \not{E}_T$ at $\sqrt{s} = 8$ TeV after each cut.

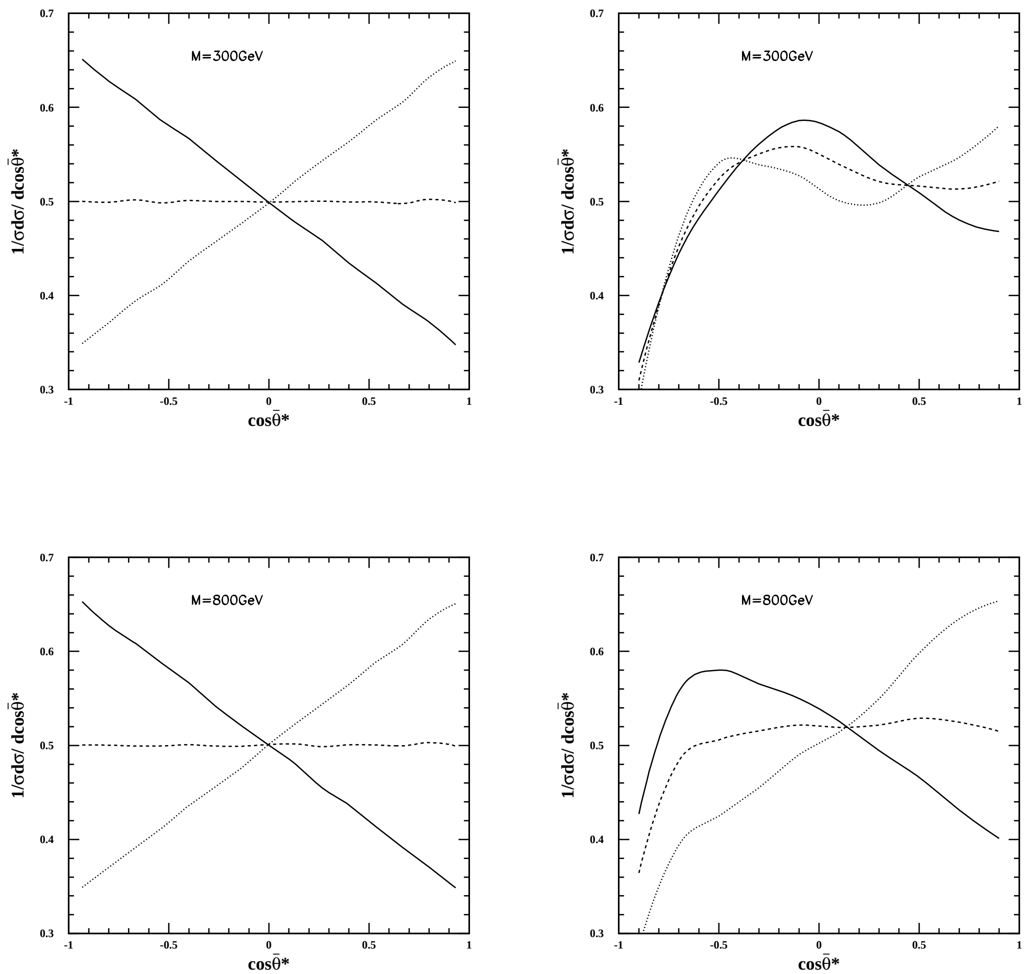

FIG. 5: The angle distribution of charged lepton for $M = 300$, 800 GeV with nocut and all cuts at $\sqrt{s} = 14$ TeV respectively for the process of $pp \to tH^- \to l^- + 5jets + \not{E}_T$.The solid line represents $(g_a g_b) > 0$. The dashed line represents $(g_a g_b) = 0$. The dotted line represents $(g_a g_b) < 0$.

Signal	$\sigma(pp \to tH^- \to t\bar{t}b \to l^\pm + 5jets + \not{E}_T)$ (fb)			
M(TeV)	0.3	0.5	0.8	1.0
No cuts	262.82	65.96	11.56	4.28
Cut I	65.79	16.41	2.75	0.95
+Cut II	54.12	13.00	2.20	0.77
+Cut III	32.47	7.80	1.32	0.46
Background	$\sigma(pp \to t\bar{t}j \to l^\pm + 5jets + \not{E}_T)$ (fb)			
Cuts I+II+III	43.54	18.97	5.95	3.22
S/B	0.75	0.41	0.22	0.14
$S/\sqrt{B}$	85.23	31.02	9.37	4.44

TABLE II: The cross section of the signal process $pp \to tH^- \to l^\pm + 5jets + \not{E}_T$ and the background process of $pp \to t\bar{t}j \to l^\pm + 5jets + \not{E}_T$ at $\sqrt{s} = 14$ TeV after each cut.

	A_{FB}				$\bar{A}_{FB}$			
without cuts								
M(TeV)	0.3	0.5	0.8	1.0	0.3	0.5	0.8	1.0
$(g_a g_b) > 0$	0.124	0.075	0.023	-0.003	-0.173	-0.173	-0.172	-0.173
$(g_a g_b) = 0$	0.0	0.0	0.0	0.0	0.0	0.0	0.0	0.0
$(g_a g_b) < 0$	-0.125	-0.076	-0.024	0.001	0.172	0.173	0.174	0.173
with cuts								
$(g_a g_b) > 0$	0.002	-0.015	-0.031	-0.041	-0.014	-0.050	-0.054	-0.061
$(g_a g_b) = 0$	-0.028	-0.030	-0.033	-0.041	-0.022	0.007	0.006	-0.006
$(g_a g_b) < 0$	-0.056	-0.048	-0.037	-0.040	-0.033	0.081	0.077	0.065

TABLE III: The forward-backward asymmetry $A_{FB}(\bar{A}_{FB})$ for $pp \to tH^- \to l^+(l^-) + 5jets + \not{E}_T$ at LHC $\sqrt{s} = 14$ TeV before and after all cuts.

Acknowledgements

This work was supported in part by the National Science Foundation of China (NSFC), Natural Science Foundation of Shandong Province(JQ200902). The authors would like to thank Dr. S. Bao, Profs. S. Li and X. He for their helpful discussions.

[1] G. Aad *et al.* [ATLAS Collaboration], Phys. Lett. B **716**, 1 (2012) [arXiv:1207.7214 [hep-ex]].
[2] S. Chatrchyan *et al.* [CMS Collaboration], Phys. Lett. B **716**, 30 (2012) [arXiv:1207.7235 [hep-ex]].
[3] S. Chang, S. K. Kang, J. -P. Lee, K. Y. Lee, S. C. Park and J. Song, arXiv:1210.3439 [hep-ph].
[4] J. F. Gunion, H. E. Haber, G. L. Kane and S. Dawson, Front. Phys. **80**, 1 (2000).
[5] G. C. Branco, P. M. Ferreira, L. Lavoura, M. N. Rebelo, M. Sher and J. P. Silva, Phys. Rept. **516**, 1 (2012) [arXiv:1106.0034 [hep-ph]].
[6] [LEP Higgs Working Group for Higgs boson searches and ALEPH and DELPHI and L3 and OPAL Collaborations], hep-ex/0107031.
[7] A. Abulencia *et al.* [CDF Collaboration], Phys. Rev. Lett. **96**, 042003 (2006) [hep-ex/0510065]; V. M. Abazov *et al.* [D0 Collaboration], Phys. Lett. B **682**, 278 (2009) [arXiv:0908.1811 [hep-ex]]; T. Aaltonen *et al.* [CDF Collaboration], Phys. Rev. Lett. **103**, 101803 (2009) [arXiv:0907.1269 [hep-ex]]; V. M. Abazov *et al.* [D0 Collaboration], Phys. Rev. D **80**, 051107 (2009) [arXiv:0906.5326 [hep-ex]].
[8] O. Deschamps, S. Descotes-Genon, S. Monteil, V. Niess, S. T'Jampens and V. Tisserand, Phys. Rev. D **82**, 073012 (2010) [arXiv:0907.5135 [hep-ph]].
[9] V. D. Barger, M. S. Berger and R. J. N. Phillips, Phys. Rev. Lett. **70**, 1368 (1993) [hep-ph/9211260].
[10] J. Beringer *et al.* [Particle Data Group Collaboration], Phys. Rev. D **86**, 010001 (2012).
[11] E. Eichten, I. Hinchliffe, K. D. Lane and C. Quigg, Rev. Mod. Phys. **56**, 579 (1984) [Addendum-ibid. **58**, 1065 (1986)]. N. G. Deshpande, X. Tata and D. A. Dicus, Phys. Rev. D **29**, 1527 (1984). S. S. D. Willenbrock, Phys. Rev. D **35**, 173 (1987). A. Krause, T. Plehn, M. Spira and P. M. Zerwas, Nucl. Phys. B **519**, 85 (1998) [hep-ph/9707430].
[12] A. A. Barrientos Bendezu and B. A. Kniehl, Phys. Rev. D **59**, 015009 (1999) [hep-ph/9807480]; S. Moretti and K. Odagiri, Phys. Rev. D **59**, 055008 (1999) [hep-ph/9809244]; S. -S. Bao, X. Gong, H. -L. Li, S. -Y. Li and Z. -G. Si, Phys. Rev. D **85** (2012) 075005 [arXiv:1112.0086 [hep-ph]].
[13] J. F. Gunion, H. E. Haber, F. E. Paige, W. -K. Tung and S. S. D. Willenbrock, Nucl. Phys. B **294**, 621 (1987). R. M. Barnett, H. E. Haber and D. E. Soper, Nucl. Phys. B **306**, 697 (1988). F. I. Olness and W. -K. Tung, Nucl. Phys. B **308**, 813 (1988).
[14] V. D. Barger, R. J. N. Phillips and D. P. Roy, Phys. Lett. B **324**, 236 (1994) [hep-ph/9311372]; J. F. Gunion, Phys. Lett. B **322**, 125 (1994) [hep-ph/9312201];
[15] D. J. Miller, 2, S. Moretti, D. P. Roy and W. J. Stirling, Phys. Rev. D **61**, 055011 (2000) [hep-ph/9906230];
[16] S. Moretti, D.P. Roy, Phys. Lett. B **470**, 209 (1999) [hep-ph/9909435];
[17] S. Moretti, K. Odagiri, Phys. Rev. D **55**, 5627 (1997) [hep-ph/9611374]; C. S. Huang and S. -H. Zhu, Phys. Rev. D **60**, 075012 (1999) [hep-ph/9812201].
[18] N. Kidonakis, JHEP **0505**, 011 (2005) [hep-ph/0412422].
[19] S. Yang and Q. -S. Yan, JHEP **1202**, 074 (2012) [arXiv:1111.4530 [hep-ph]].
[20] S. Gopalakrishna, T. Han, I. Lewis, Z. G. Si and Y. -F. Zhou, Phys. Rev. D **82**, 115020 (2010) [arXiv:1008.3508 [hep-ph]].
[21] F. Mahmoudi and O. Stal, Phys. Rev. D **81**, 035016 (2010) [arXiv:0907.1791 [hep-ph]].

[22] J. L. Hewett, Phys. Rev. Lett. **70**, 1045 (1993) [arXiv:hep-ph/9211256].
[23] V. D. Barger, M. S. Berger and R. J. N. Phillips, Phys. Rev. Lett. **70**, 1368 (1993) [arXiv:hep-ph/9211260].
[24] S. Bertolini, F. Borzumati, A. Masiero and G. Ridolfi, Nucl. Phys. B **353**, 591 (1991).
[25] A. Brandenburg, Z. G. Si and P. Uwer, Phys. Lett. B **539**, 235 (2002) [hep-ph/0205023]. A. Czarnecki, M. Jezabek and J. H. Kuhn, Nucl. Phys. B **351**, 70 (1991).
[26] J. Pumplin, D. R. Stump, J. Huston, H. L. Lai, P. M. Nadolsky and W. K. Tung, JHEP **0207**, 012 (2002) [arXiv:hep-ph/0201195].
[27] G. Aad *et al.* [ATLAS Collaboration], arXiv:0901.0512 [hep-ex].
[28] J. Alwall, M. Herquet, F. Maltoni, O. Mattelaer and T. Stelzer, JHEP **1106**, 128 (2011) [arXiv:1106.0522 [hep-ph]].
[29] W. Bernreuther, A. Brandenburg, Z. G. Si and P. Uwer, Nucl. Phys. B **690** (2004) 81 [hep-ph/0403035]. W. Bernreuther, A. Brandenburg, Z. G. Si and P. Uwer, Phys. Rev. Lett. **87** (2001) 242002 [hep-ph/0107086].
[30] W. Bernreuther and Z. -G. Si, Nucl. Phys. B **837** (2010) 90 [arXiv:1003.3926 [hep-ph]].